0026-895X/11/8001-97–109$25.00
MOLECULAR PHARMACOLOGY
Vol. 80, No. 1
71308/3698101
Mol Pharmacol 80:97–109, 2011
Printed in U.S.A.

Abelson Family Tyrosine Kinases Regulate the Function of Nicotinic Acetylcholine Receptors and Nicotinic Synapses on Autonomic Neurons[S]

Selwyn S. Jayakar and Joseph F. Margiotta

Department of Neurosciences, University of Toledo College of Medicine, Toledo, Ohio

Received January 21, 2011; accepted April 18, 2011

ABSTRACT

Abelson family kinases (AFKs; Abl1, Abl2) are non-receptor tyrosine kinases (NRTKs) implicated in cancer, but they also have important physiological roles that include regulating synaptic structure and function. Recent studies using Abl-deficient mice and the antileukemia drug STI571 [imatinib mesylate (Gleevec); Novartis], which potently and selectively blocks Abl kinase activity, implicate AFKs in regulating presynaptic neurotransmitter release in hippocampus and postsynaptic clustering of nicotinic acetylcholine receptors (nAChRs) in muscle. Here, we tested whether AFKs are relevant for regulating nAChRs and nAChR-mediated synapses on autonomic neurons. AFK immunoreactivity was detected in ciliary ganglion (CG) lysates and neurons, and STI571 application blocked endogenous Abl tyrosine kinase activity. With similar potency, STI571 specifically reduced whole-cell current responses generated by both nicotinic receptor subtypes present on CG neurons (α3*- and α7-nAChRs) and lowered the frequency and amplitude of α3*-nAChR-mediated excitatory postsynaptic currents. Quantal analysis indicated that the synaptic perturbations were postsynaptic in origin, and confocal imaging experiments revealed they were unaccompanied by changes in nAChR clustering or alignment with presynaptic terminals. The results indicate that in autonomic neurons, Abl kinase activity normally supports postsynaptic nAChR function to sustain nAChR-mediated neurotransmission. Such consequences contrast with the influence of Abl kinase activity on presynaptic function and synaptic structure in hippocampus and muscle, respectively, demonstrating a cell-specific mechanism of action. Finally, because STI571 potently inhibits Abl kinase activity, the autonomic dysfunction side effects associated with its use as a chemotherapeutic agent may result from perturbed α3*- and/or α7-nAChR function.

Introduction

Nicotinic acetylcholine receptors (nAChRs) are critical components of synapses throughout the nervous system. In autonomic ganglia, peri- and postsynaptic nAChRs mediate excitatory neurotransmission and presynaptic nAChRs regulate acetylcholine release, whereas in brain, peri- and presynaptic nAChRs modulate neurotransmitter efficacy and release, respectively (Margiotta and Pugh, 2004). Consistent with their diversity and widespread distribution, nAChRs are involved in several neurological disorders. Autonomic ganglia feature nAChRs assembled from α7 subunits (α7-nAChRs) and from α3, β4, α5 $\pm$ β2 subunits (α3*-nAChRs) (Margiotta and Pugh, 2004), and a constellation of ganglionopathies are associated with the presence of α3 subunit autoantibodies that impair

This work was supported by the National Institutes of Health National Institute on Drug Abuse [Grant R01-DA015536, R21-DA022280] (to J.F.M.); and by the National Science Foundation Division of Integrative Organismal Systems [Grant 0951549] (to J.F.M.).

Article, publication date, and citation information can be found at http://molpharm.aspetjournals.org.

doi:10.1124/mol.111.071308.

[S] The online version of this article (available at http://molpharm.aspetjournals.org) contains supplemental material.

ABBREVIATIONS: nAChR, nicotinic acetylcholine receptor; α7-nAChR, nAChR assembled from α7 subunits; α3*-nAChR, nAChR assembled from α3, β4, α5 $\pm$ β2 subunits; AFK, Abelson family tyrosine kinase; Abl1, c-Abl, Abelson family tyrosine kinase 1; Abl2, Arg, Abelson family tyrosine kinase 2; CML, chronic myeloid leukemia; STI571, imatinib mesylate; MuSK, muscle-specific kinase; NRTK, nonreceptor tyrosine kinase; CG, ciliary ganglion; E, embryonic day; RS, recording solution; RS^{hs}, recording solution supplemented with 10% heat-inactivated horse serum; GTS-21, 3-(2,4-dimethoxybenzylidene)anabaseine; αBgt, α-bungarotoxin; sEPSC, spontaneous excitatory postsynaptic current; eEPSC, evoked excitatory postsynaptic current; mEPSC, miniature excitatory postsynaptic current; TTX, tetrodotoxin; PBS, phosphate-buffered saline; BS/TX, block solution containing PBS with 5% normal goat serum and 0.1% TX-100; WS, wash solution; PDGF, platelet-derived growth factor; NGS, normal goat serum; BSA, bovine serum albumin; SV2, synaptic vesicle protein 2; ROI, region of interest; TB, Tris-Triton buffer; PAGE, polyacrylamide gel electrophoresis; mAb, monoclonal antibody; pAb, polyclonal antibody; HRP, horseradish peroxidase; AU, arbitrary units; PDGF, platelet-derived growth factor; PDGFR, PDGF receptor; SCF, stem cell factor; c-Kit, stem cell factor receptor; PSD, postsynaptic density; CRIPT, cysteine rich PDZ binding protein; PTPase, protein-tyrosine phosphatase.

receptor function and synaptic transmission (Vernino et al., 2009). In brain, nAChRs containing $\alpha4$ and $\beta2$ subunits ($\alpha4\beta2$-nAChRs) have been in implicated in Alzheimer's disease, Parkinson's disease, and schizophrenia (Newhouse and Kelton, 2000). Moreover, brain $\alpha4\beta2$-nAChR up-regulation caused by long-term nicotine exposure is likely to underlie nicotine dependence in smokers (Nashmi et al., 2007). Thus, pharmacological agents that perturb nAChRs are of interest for understanding synapses and as potential therapeutic agents for combating neurological disease and nicotine addiction.

Abelson family kinases (AFKs; Abl1 and Abl2) interact with kinases, phosphatases, signaling adaptors, and scaffolding proteins (Pendergast, 2002). Abl1 (c-Abl) and its paralog Abl2 (Arg) feature a conserved tyrosine kinase domain, upstream SH2 and SH3 domains, a variable upstream "Cap" region that acts with SH domains to inhibit autophosphorylation, and a C-terminal actin-binding domain. Chromosomal translocation induces BCR-Abl, an oncogenic fusion protein that has disinhibited Abl kinase activity linked to chronic myeloid leukemia (CML) (Sirvent et al., 2008). Abl kinase activity is selectively blocked by STI571 [imatinib mesylate (Gleevec); Novartis, Basel, Switzerland], a rationally designed anticancer drug inducing complete albeit transient remission (Corbin et al., 2002). AFKs also mediate cell adhesion, shape, and movement via kinase-independent interaction with the F-actin cytoskeleton (Wang et al., 2001; Pendergast, 2002) and contribute to neural development and synaptic structure/function. Abl2 is abundant at synapse-rich regions of the cerebellum, olfactory bulb and hippocampus, and *Abl1*(−/−)*Abl2*(−/−) mice embryos display neural tube collapse (Koleske et al., 1998). Moreover, although brains of *Abl2*(−/−) mice appear normal, behavioral impairments suggest an impact on synaptic function (Koleske et al., 1998). In hippocampus, Abl1 modulates neurotransmitter release (Moresco et al., 2003), colocalizes with PSD-95, and regulates its clustering by tyrosine phosphorylation (de Arce et al., 2010), effects that are all blocked by Abl kinase inhibition with STI571. It is noteworthy that both Abl1 and Abl2 are expressed at the mouse neuromuscular junction, and experiments with STI571 indicate that reciprocal phosphorylation of Abl and muscle-specific kinase (MuSK) is required for agrin-induced nAChR clustering (Finn et al., 2003). Although MuSK and agrin are present in the nervous system, their signaling outcomes are distinct from those in skeletal muscle (Hilgenberg and Smith, 2004; Garcia-Osta et al., 2006). Neuronal nAChRs, however, are tightly regulated by phosphorylation via serine/threonine kinases and tyrosine kinases, including receptor tyrosine kinases (e.g., TrkB) (Pardi and Margiotta, 1999; Zhou et al., 2004) and NRTKs. NRTK inhibition with herbimycin A alters the number and composition of $\alpha3$*-nAChRs in chick ciliary ganglion (CG) neurons (Haselbeck and Berg, 1996). In chromaffin cells, inhibiting Src-family NRTKs reduced $\alpha3$*-nAChR currents, and inhibiting tyrosine phosphatase activity reversed the effect (Wang et al., 2004) whereas in hippocampal neurons, where $\alpha7$-nAChRs are tyrosine-phosphorylated, the opposite effects are observed (Charpantier et al., 2005). Despite the importance of AFKs in neuromuscular junction formation, CNS development, and synapses, and the relevance of tyrosine phosphorylation to nicotinic signaling, the role of Abl tyrosine kinase activity in regulating neuronal nAChRs and nicotinic synapses has not been explored.

To determine whether AFKs influence neuronal nAChR function and nAChR-mediated synapses, we used STI571 to block their endogenous kinase activity in the CG system. The system is ideal for such studies because CG neurons express functionally distinguishable $\alpha3$*- and $\alpha7$-nAChR subtypes (Nai et al., 2003) and form accessible $\alpha3$*-nAChR-mediated interneuronal synapses in cell culture (Chen et al., 2001; Pugh et al., 2010). We find that AFKs are expressed in CG extracts and neurons and that STI571 treatment blocks their endogenous tyrosine kinase activity. Unlike its actions on nAChR clustering in muscle or synaptic structure and presynaptic function in brain, however, STI571 had no effect on nAChR receptor clustering, synaptic localization, or presynaptic quantal content. Instead, it rapidly, potently, and specifically impaired $\alpha3$*- and $\alpha7$-nAChR function and thus inhibited subsequent nAChR-mediated postsynaptic transmission by reducing quantal size. These actions indicate that AFKs are part of a novel signaling pathway in autonomic neurons that normally sustains the function of nAChRs, including those at postsynaptic sites.

Materials and Methods

Neuron Preparations

CG neurons were dissociated from embryonic day 14 (E14; stage 40) chick ciliary ganglia using collagenase A treatment and mechanical trituration procedures as described previously (Nai et al., 2003). The neurons were suspended in a recording solution (RS) containing 145.0 mM NaCl, 5.3 mM KCl, 0.8 mM Mg_2SO_4, 5.4 mM $CaCl_2$, 5.6 mM glucose, and 5.0 mM HEPES acid, pH 7.4, that was supplemented with 10% heat-inactivated horse serum (RS^{hs}). Neurons were plated on 12-mm diameter glass coverslips (Thermo Fisher Scientific, Waltham, MA) coated with 300-kDa poly-D-lysine (2 mg/ml; Sigma-Aldrich, St. Louis, MO) at 1.5 CG equivalents ($\approx 4.5 \times 10^3$ neurons) per coverslip. The neurons were allowed to attach to the substrate for 30 min at room temperature (21°C) and then equilibrated for 1.5 h at 37°C before use in experiments.

CG neuron cultures were prepared and maintained under sterile conditions as described previously (Chen et al., 2001; Zhou et al., 2004; Pugh et al., 2010). In brief, 12-mm diameter glass coverslips were coated with poly-DL-ornithine (0.2 mg/ml; Sigma-Aldrich) for 14 to 16 h and then coated with laminin (5 μg/ml; BD Biosciences, San Jose, CA) for 2 to 3 h. E8 (stage 34–35) ciliary ganglia were treated with trypsin-EDTA (0.25 mg/ml; Invitrogen, Carlsbad, CA) for 8 to 10 min followed by mechanical trituration, and the dissociated neurons were plated at 1.5 ganglion equivalents per coverslip. Cultures were maintained in 16-mm-well plates at 37°C in a humidified atmosphere of 95% air/5% CO_2 and received fresh culture medium every 2 days. The complete culture medium consisted of Eagle's minimum essential medium that was supplemented with 100 U/ml penicillin, 100 mg/ml streptomycin, 2 mM glutamine, 10% heat-inactivated horse serum (all components from Invitrogen), and 3% freshly prepared E17 chick eye extract. Depending on the neuron preparation, treatments with STI571 or other reagents were made at 37°C in either RS^{hs} or culture medium for times indicated under *Results*.

Electrophysiology

Whole-cell recordings were obtained at 21°C from CG neurons dissociated at E14 or maintained in culture. The neurons were bathed in RS^{hs} ± STI571 or other reagents as indicated under *Results*. Patch pipettes were pulled from Corning 8161 glass tubing (Warner Instruments, Hamden, CT), filled with an intracellular solution containing 145.6 mM CsCl, 1.2 mM $CaCl_2$, 2.0 mM EGTA, 15.4 mM glucose, and 5.0 mM Na-HEPES, pH 7.3, and had tip impedances of 2 to 4 MΩ. Membrane currents were recorded in the whole-cell configuration at

−70 mV and low-pass-filtered at 2 to 10 kHz using an Axopatch 200B patch clamp in combination with a Digidata 1322A interface controlled by pClamp 9.0 software (all from Molecular Devices, Sunnyvale, CA), and stored on a desktop computer. Upon establishing the whole-cell recording configuration, input and series resistances were measured, and membrane capacitance (C_m) compensation was applied. Voltage-activated Na^+ and Ca^{2+} currents were acquired by applying a family of 17.5-ms command depolarizations from the holding potential (−70 mV). Series resistance values were typically <10 MΩ, and no correction was applied. Neurons displaying series resistances >15 MΩ, input impedances <300 MΩ, or peak Na^+ currents <3 nA were excluded from analysis. α7-nAChR responses were selectively induced using 3-(2,4-dimethoxybenzylidene)anabaseine (GTS-21), whereas α3*-nAChR responses were isolated using nicotine applied in the presence of 50 nM α-bungarotoxin (αBgt), both as described previously (Nai et al., 2003). The agonists were dissolved in RS (with or without αBgt) at the desired final concentration from frozen aqueous stocks (2 mM nicotine and 10 mM GTS-21). Agonists were focally applied to individual neuron somas (held at −70 mV) delivered from 4- to 6-μm diameter patch pipettes (Microhematocrit; VWR Scientific Inc., West Chester, PA) by microperfusion (5.0–7.5 psi) using a computer-triggered pressure valve (Picospritzer II; General Valve Co., Fairfield, NJ). Whole-cell currents induced by nAChR agonists were analyzed offline using Clampfit software (pClamp 9.0). To normalize for size differences in neuron somas, having capacitances of 15 to 30 pF, peak agonist-induced current amplitudes (I_{peak}) were divided by soma membrane capacitance (C_m) such that specific responses are expressed as peak current densities (picoamperes per picofarad). To assess synaptic function in CG cultures, spontaneous, impulse-dependent excitatory postsynaptic currents (sEPSCs) or quantal, impulse-independent, miniature EPSCs (mEPSCs) were acquired for 120 s from neurons held at −70 mV without or with TTX (1 μM) pretreatment, respectively, as described previously (Chen et al., 2001; Pugh et al., 2010). Spontaneous synaptic currents having amplitudes >3 × root-mean-square noise were analyzed off-line using Mini Analysis software (version 6.0.3; Synaptsoft) as described previously (Zhou et al., 2004; Pugh et al., 2010). In some experiments, EPSCs were evoked by stimulating neurite fascicles that converge on target neurons using bipolar stimulating electrodes fabricated from θ-shaped glass tubing (Warner Instruments) as described previously (Pugh et al., 2010). While target neurons were held in whole-cell mode, convergent neurite fascicles were partially drawn into the electrode barrels by applying gentle suction. Voltage pulses (0.1–0.3 ms) were then applied using an isolated bipolar stimulator (model 2100; A-M Systems, Carlsborg, WA) with the intensity adjusted to activate single axons (Pugh et al., 2010). Average evoked EPSC (eEPSC) amplitudes were obtained for each trial by dividing the sum of all event amplitudes (including failures) by the total number of applied stimuli (between 30 and 230 at 0.5 Hz). Results are expressed both as raw means and as parameter values normalized to the control condition for each experiment. The statistical significance of differences between results for control and test conditions ($p < 0.05$) was determined using Student's unpaired two-tailed t-test, with correction for unequal variances applied where applicable (Prism 4; GraphPad Software, San Diego, CA).

Imaging

Immunolabeling. Protein localization was assessed by fluorescence immunolabeling, image acquisition, and analysis using CG neurons on glass coverslips, either grown in culture for 4 days or acutely dissociated at E14. To label AFKs, neurons were brought to room temperature (21°C) washed in 0.1 M phosphate-buffered saline (PBS, pH 7.4; 2 min) and fixed (4% paraformaldehyde in PBS, 20 min). Fixed neurons were washed with PBS (3×, 5 min), blocked, permeabilized in block solution containing PBS with 5% normal goat serum and 0.1% TX-100 (BS/TX) for 1 h, and incubated in BS/TX containing rabbit Anti-Abl polyclonal antibody K-12 (pAbK-12; 1:2000) raised against a peptide mapping within the kinase domain of human Abl1 (Santa Cruz Biotechnology Inc., Santa Cruz, CA) for 16 h, at 4°C. Because the kinase domains of Abl1 and Abl2 are 94% identical (Pendergast, 2002), pAbK-12 is also likely to react with Abl2. Neurons were then brought to 21°C, washed in a solution containing PBS with 0.1% Triton X-100 (WS; 3×, 5 min), incubated in BS/TX containing Alexa Fluor 488 conjugated mouse anti-rabbit secondary antibody (1:400, 1 h; Invitrogen), washed again in WS (3×, 5 min), then in PBS (1×, 5 min). A similar procedure was followed to detect platelet-derived growth factor (PDGF) receptors using an anti-PDGFR pAb (1:100) that recognizes both PDGF-α and -β receptors (Cell Signaling Technology, Danvers, MA).

To label α3*-nAChRs, neurons were brought to room temperature (21°C), washed in RS^{hs} (2×, 5 min), and incubated with mAb35 (anti-α3/α5-nAChR subunit, 1:500; a gift from Dr. D. K. Berg, University of California, San Diego, CA) in RS^{hs} containing 17% NGS (RS^{hs}/NGS, 1.5 h, 21°C) and washed in RS^{hs} (3X, 5 min), incubated in Cy3-conjugated secondary antibody (1:200, in RS/NGS, 2 h, 21°C; Jackson ImmunoResearch Laboratories), and washed in RS^{hs} (2×, 5 min) then in PBS (3×, 5 min). To label α7-nAChRs, neurons were washed in RS containing 2 mg/ml bovine serum albumin (RS/BSA, 2×, 5 min; BSA from Thermo Fisher Scientific) and incubated with Alexa Fluor 488-conjugated αBgt (Bgt-AF488, 1:400; Invitrogen) in RS/BSA for 30 min at 37°C and washed in PBS (3×, 5 min). In both cases, the neurons were then fixed (2–4% paraformaldehyde in PBS, 20 min) and washed in PBS (3×, 5 min).

To colabel α3*-nAChRs and synaptic vesicle protein 2 (SV2), CG cultures were incubated with mAb35 as above and then washed (WS, 3×, 5 min), fixed (2% paraformaldehyde, 20 min), blocked, permeabilized (BS/TX, 1 h), and incubated with anti-SV2 mAb10h (1:25; Developmental Studies Hybridoma Bank, University of Iowa, Iowa City, IA) in BS/TX (16 h at 4°C). They were then washed (WS, 3×, 5 min), incubated with Alexa Fluor 488-conjugated mouse (1:400) and Cy3-conjugated rat secondary antibodies (1:200, 1 h in BS/TX; Jackson ImmunoResearch Laboratories), washed (WS, 3×, 5 min), and then rinsed in PBS (1×, 5 min). In all cases, coverslips were mounted on glass slides in Vectashield (Vector Laboratories, Burlingame, CA).

Image Acquisition and Analysis. Toxin and antibody-labeled neurons were examined using a 60× (1.2 numerical aperture, UPlanApo) objective on an Olympus BX51WI fixed-stage microscope (Olympus America Inc., Center Valley, PA) equipped with a Radiance2000 laser-scanning confocal imaging system (Bio-Rad Laboratories, Hercules, CA) and LaserSharp2000 software controlling argon (488 nm) and green helium neon (543 nm) lasers (Carl Zeiss MicroImaging). For each neuron, sequential eight-bit images were acquired at 512 × 512 (0.1559 μm/pixel) x-y resolution, and 20 to 30 optical z-sections (0.5–1.0 μm thick) were collected using a motorized focus unit (0.05 μm resolution; Bio-Rad Laboratories). Laser power and gain were set to minimize saturation and avoid detectable bleed-through between the channels. To enable comparison of control and test conditions, exposure settings were held constant within a given experiment. Image stacks were saved as TIFF files and analyzed with the use of ImageJ (http://rsbweb.nih.gov/ij/).

To assess synaptic localization, sequential confocal image stacks were acquired from CG neurons colabeled with mAb35 and mAbh10 to detect α3*-nAChRs and SV2-containing presynaptic terminals, respectively. For each neuron analyzed, a single upper *en face* (surface) z-section (or a projection from one to two two adjacent sections) was identified, and a region of interest (ROI) was drawn to surround the extent of detectable labeling on the α3 image and copied to the SV2 image. α3*-nAChR (and SV2) labeling intensity was obtained from the mean fluorescence intensity within the ROI minus the mean background fluorescence outside the ROI ($\Delta F = F_m - F_b$) divided by F_b ($\Delta F/F_b$). α3*-nAChR and SV2 clusters (at least two adjacent pixels; 48.6 nm^2) were quantified by establishing a threshold (8–10 × F_b) and their densities (number per square micrometer), areas (square nanometer), and intensities ($\Delta F/F_b$) determined after automated particle counting. The extent of α3*-nAChR and SV2

colocalization was assessed from Manders' coefficients (R_M), which have values of 0 to 1 indicative of perfect exclusion and overlap, respectively. Portions of α3*-nAChR clusters that mapped to adjacent SV2 clusters were considered postsynaptic, and the densities, areas, and relative intensities of these synaptic α3*-nAChR puncta were quantified as above for α3*-nAChR clusters.

Immunoprecipitation and Immunoblotting

For biochemical detection, proteins were first immunoprecipitated from E14 CG lysates. Frozen ganglia (40 CGs at −80°C) were thawed on ice and homogenized using a tissue homogenizer (0.1 ml; Wheaton, Millville, NJ) in 2 ml of Tris-Triton buffer (TB) containing 50 mM Tris, pH 7.4, 0.5% Triton X-100, and protease inhibitor cocktail (1:200; Sigma-Aldrich), and solubilized in TB for 1 h at 4°C with mixing. Insoluble material was removed by centrifugation (20,000*g*, 15 min, 4°C), and the lysates were precleared with protein A/G beads (20 μl, washed 2× in PBS, 21°C; Thermo Fisher Scientific) for 30 min at 4°C with mixing. For AFKs, lysates (1 ml each) were incubated without or with pAbK-12 (1:200) at 4°C for 1 h with mixing. Protein A/G beads (20 μl washed 2× in PBS, 21°C) were then incubated with precleared lysates for 1 h with mixing. The beads were allowed to settle (5 min, on ice) and washed with TB (6×, 1 ml per wash, on ice) after the lysate was removed. Material bound to the beads was eluted with SDS-PAGE sample buffer (50 μl, 21°C) subjected to SDS-PAGE (120 V, 2 h), electroblotted to nitrocellulose (100 V, 2 h), and probed with anti-Abl monoclonal antibody 8E9 (mAb8E9; 1:500; BD Biosciences) followed by HRP-conjugated anti-mouse secondary antibodies (1:5000; Jackson ImmunoResearch Laboratories). Because mAb8e9 recognizes an epitope within the kinase domain of Abl1 that shares 94% identity with Abl2 (Pendergast, 2002), it was expected to recognize both Abl proteins. A similar procedure was followed to detect PDGF receptors using an anti-PDGFR pAb that recognizes both PDGF-α and -β receptors (Cell Signaling Technology) for both immunoprecipitation (1:50) and probing (1:1000). Signals were visualized by enhanced chemiluminescence (Immun-Star HRP Substrate kit; Bio-Rad Laboratories).

Phosphorylation Assay

To detect phosphorylation of AFK substrate protein CrkII, E14 ciliary ganglia were incubated in RS^{hs} with or without STI571 (10 μM) for 1 h at 4°C (40 freshly dissected ganglia were used for each condition). They were then equilibrated at 21°C for 30 min, homogenized as above (1 ml for each condition) in TB containing phosphatase inhibitor cocktail (1:200; Sigma-Aldrich), and solubilized in the same solution for 1 h at 4°C with mixing. Insoluble material was removed by centrifugation (20,000*g*, 15 min, 4°C). The lysates were precleared with protein A/G beads (20 μl, washed 2× in PBS, 21°C; Thermo Fisher Scientific) for 30 min at 4°C with mixing, incubated with anti-Crk mAb (22/Crk, 1:250; BD Biosciences) for 1 h at 4°C with mixing to bind endogenous Crk protein. Protein A/G beads (20 μl, washed 2× in PBS, 21°C) were added and incubated for 1 h at 4°C with mixing. The beads were allowed to settle (5 min, on ice), and washed with TB containing phosphatase inhibitor cocktail (1:200, 6×, 1 ml per wash, on ice) after the lysate was removed. Bound material was eluted with SDS-PAGE sample buffer (50 μl, 21°C), subjected to SDS-PAGE, electrophoresed (120 V, 2 h), electroblotted to nitrocellulose (100 V, 2 h), and probed either with anti-Crk or with anti-phospho-CrkII (Tyr 221) pAb (1:1000; Cell Signaling Technology), followed by goat anti-mouse or rabbit HRP-conjugated secondary antibodies (1:5000, 1 h; Jackson ImmunoResearch), respectively. Signals were visualized by enhanced chemiluminescence (Immun-Star HRP Substrate kit; Bio-Rad Laboratories).

Materials

Fertilized white Leghorn chicken eggs were obtained from Hertzfeld Poultry Farms (Waterville, OH) and maintained at 37°C in a forced air draft incubator at 100% humidity. STI571 was a generous gift from Novartis.

Results

Abl Family Kinases Are Present in the Ciliary Ganglion

Synapse formation between preganglionic midbrain neurons and postganglionic CG neurons begins at E5 and, although functional innervation is complete by E8, the synapses mature through E14 and beyond (Dryer, 1994). Because AFKs are required to maintain nAChR clusters on skeletal myotubes (Finn et al., 2003), we speculated that their expression might change during the formation and/or maturation of neuronal nicotinic synapses. To test this idea, AFK levels were assessed in CG homogenates prepared from E6, E8, E11, and E14 embryos. After immunoprecipitation with Anti-Abl pAbK-12, immunoblotting with Anti-Abl mAb8E9 revealed an interacting protein of the predicted size (145 kDa) at each developmental stage (Fig. 1A). To quantify changes in AFK expression, band intensities (arbitrary intensity units, AU) were normalized to total protein loaded and to the number of neurons per CG at each stage. This analysis revealed a robust developmental increase in AFK expression of 2.9-fold per mg of protein (from 307 ± 101 to 877 ± 115 AU/mg, $p < 0.05$) and 5.8-fold per of neuron (from 0.0013 ± 0.0004 to 0.0076 ± 0.0009 AU/neuron, $p < 0.05$) between E6 and E14 (Fig. 1B). Because the CG contains both neurons and support cells, the cellular localization of AFKs was also examined by immunolabeling with pAbK-12. Robust cytoplasmic AFK labeling was detected in CG neurons when acutely dissociated at E14 or grown in cell culture for 4 days, but little or no labeling was detectable in non-neuronal cells (Fig. 1C). These results indicate that AFK levels increase during the developmental period of nicotinic synapse formation and maturation in the CG with robust expression in neurons.

Endogenous Abl Family Kinase Activity Is Inhibited by STI571

Endogenous Abl kinase activity was assessed by testing whether STI571 inhibited basal tyrosine kinase activity. This was accomplished by monitoring the phosphorylation levels of endogenous CrkII, a substrate specifically phosphorylated by Abl1 and Abl2 at Tyr221 (Feller et al., 1994). Crk proteins were immunoprecipitated from lysates prepared from diced sham- or STI571-treated E14 ciliary ganglia, and blots probed with anti-Crk and anti-Phospho-CrkII, the latter to detect phosphorylation at Tyr221. CrkII phosphorylation was evident in blots from control extracts indicative of considerable endogenous tyrosine kinase activity in the CG (Fig. 1D). Moreover, such CrKII phosphorylation was virtually eliminated in lysates from ganglia pretreated with STI571, indicating that the drug inhibits endogenous Abl kinase activity. As observed previously (Finn et al., 2003), Crk protein migrates as a doublet such that the more slowly migrating band, corresponding to the tyrosine-phosphorylated form, collapses into the more quickly migrating nonphosphorylated form after Abl kinase inhibition with STI571. This shift to a faster migrating species provides additional evidence supporting decreased Abl kinase activity after STI571 treatment. Together, these experiments demonstrate that STI571

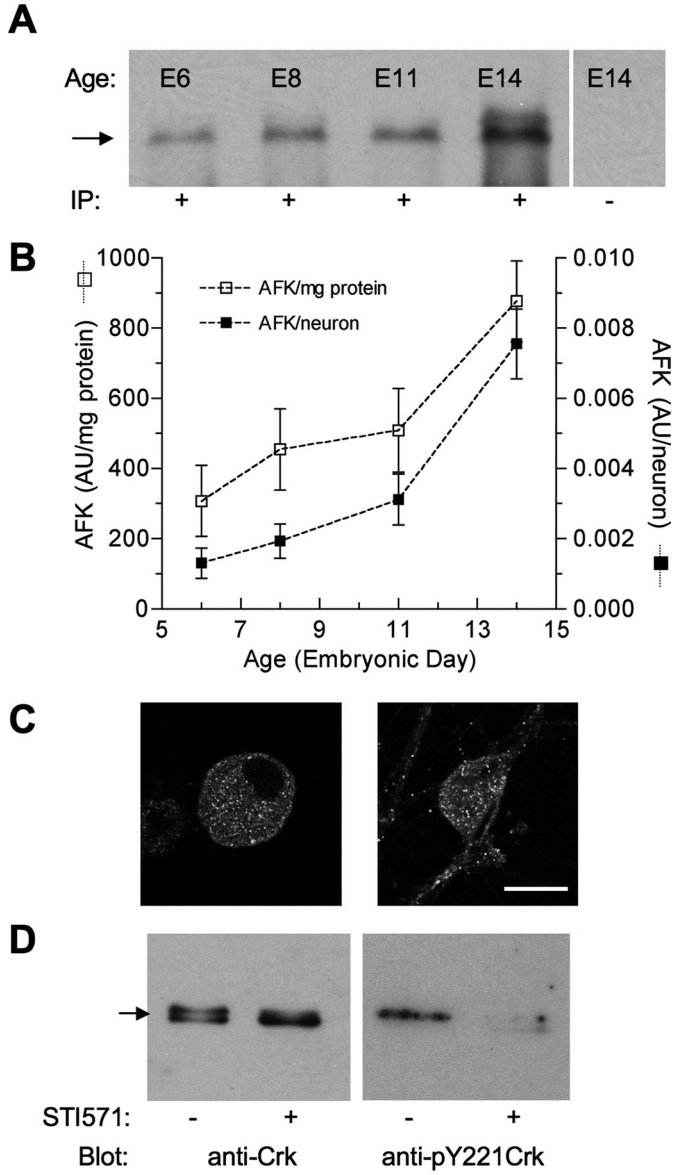

Fig. 1. AFKs are present in ciliary ganglion homogenates and neurons, and Abl kinase activity is inhibited by STI571. A, developmental expression of AFKs. Homogenates prepared from ciliary ganglia (0.15 mg/ml total protein) throughout the developmental period when nicotinic synapses form and mature (E6, -8, -11, and -14) were subjected to immunoprecipitation with (+) or without (−) anti-Abl K-12. After probing with anti-Abl mAb8E9, an interacting protein expected at ~145 kDa (arrow) was detected at each developmental age. B, quantification reveals that Abl family kinase levels progressively increase between E6 and E14. Results are expressed as band intensity (AU) per milligram of ganglionic protein loaded (□) or as band intensity per neuron at the indicated embryonic age (■) (mean ± S.D.). C, neuronal localization. Confocal images (single 1-μm optical sections) depict an acutely dissociated E14 CG neuron (left) and a CG neuron grown 4 days in culture (right) immunolabeled using anti-Abl K12 antibody and reveal a largely cytoplasmic distribution of AFKs. Control neurons (no added primary antibody) were unlabeled (data not shown). Scale bar, 15 μm. D, STI571 inhibits endogenous Abl kinase activity. E14 ciliary ganglion quadrants were pretreated with (+) or without (−) STI571 (10 μM; 30 min); lysates were then prepared, immunoprecipitated with anti-Crk, and probed either with anti-Crk (left) or anti-pY221Crk (right). Note that pTyr221 levels are undetectable in lysates from ganglia after pretreatment with STI571. Each lane represents 40 CG equivalents, or approximately 14.3 mg total protein (wet weight). The arrow indicates 37 kDa. Similar results were obtained from two other experiments.

can be used to perturb endogenous Abl kinase activity in the CG system.

Inhibiting Abl Family Kinases Reduces nAChR Responses

Because neuronal nAChRs can be regulated by tyrosine phosphorylation, we tested whether inhibiting Abl kinase activity with STI571 would influence their function (Fig. 2). At E14, CG neurons express both α3*- and α7-nAChR subtypes, which generate large, pharmacologically distinguishable responses in whole-cell current recordings (Nai et al., 2003). With αBgt present to block α7-nAChRs, focal application of nicotine (20 μM) induces whole-cell currents in CG neurons that are mediated solely by α3*-nAChRs (Nai et al., 2003). STI571 (10 μM) reduced peak α3*-nAChR current responses (I^*_{peak}) by ≈60% relative to sham-treated controls within 1 h, a level of inhibition that was not exceeded after longer treatments up to 7 h (Fig. 2A). The STI571-mediated reduction of α3*-nAChR responses was dose-dependent, with maximum inhibition observed at 3 μM STI571 and a predicted IC_{50} of 0.6 μM (Fig. 2C). Similar results were obtained using GTS-21 (30 μM) to selectively activate α7-nAChRs (Nai et al., 2003). Here, STI571 (10 μM) stably reduced peak GTS-21 induced α7-nAChR-mediated currents by ≈60% within 1 h, and maximal inhibition was achieved at 3 μM and a predicted IC_{50} of 0.7 μM STI571 (Fig. 2, B and D). The nAChR inhibition constants are consistent with those obtained for STI571 inhibition of Abl kinase activity (0.1–0.5 μM) (Okuda et al., 2001; Capdeville et al., 2002). STI571 reduced α3*- and α7-nAChR current amplitudes without appreciably affecting response kinetics (Table 1). In particular, the desensitization time constants associated with α3*- and α7-nAChR responses were unchanged by STI571. Likewise, STI571 treatment failed to change the time to achieve peak (T_{peak}) α3*-nAChR responses, and only slightly increased T_{peak} for α7-nAChR responses. Moreover, the ability of STI571 to inhibit nAChR responses was specific because it failed to change GABA receptor responses induced by 25 μM GABA when focally applied in the same fashion or to alter Na^+ or Ca^{2+} channel currents evoked by applying depolarizing voltage steps (data not shown). These results demonstrate that STI571 rapidly and stably reduces peak α3*- and α7-nAChR current responses at potencies consistent with Abl kinase inhibition and does so without affecting nAChR activation or desensitization kinetics, or other channel types.

Inhibiting Abl Family Kinases Reduces nAChR-Mediated Synaptic Activity

Because Abl kinase inhibition selectively reduced α3*- and α7-nAChR currents, it should also influence nAChR-mediated synaptic function. This idea was tested in CG cultures in which spontaneously active nicotinic synapses form between the neurons, and virtually all transmission is mediated by α3*-nAChRs (Chen et al., 2001). The cultures present a useful model system for examining regulatory influences on nicotinic synapses, because pre- and postsynaptic components of transmission can be accessed and their respective functional contributions tested (Pugh et al., 2010). Similar to its effects on acutely dissociated E14 neurons (Fig. 2), STI571 reduced peak α3*-nAChR responses in 4-day CG cultures to 44 ± 9% (n = 6) of those from control CG neurons tested in parallel (n = 6; $p < 0.001$; data not shown). Consistent with this action, Abl kinase inhibition depressed synaptic activity,

as seen by reductions in the frequency and amplitude of α3*-nAChR mediated spontaneous excitatory postsynaptic currents (sEPSCs) (Fig. 3A). In individual experiments from 4-day CG cultures, sEPSC frequencies (F_s) and amplitudes (A_s) were distributed with overall means of 0.83 ± 0.12 Hz and −27.8 ± 1.5 pA, respectively, similar to values we reported previously (Chen et al., 2001; Pugh et al., 2010). STI571 (10 μM, 1 and 24 h combined) left-shifted the distributions (Fig. 3, B and C), and the overall means of F_s and A_s were significantly reduced to 0.28 ± 0.05 Hz and −11.9 ± 1.3 pA (Table 2), representing 27 and 47% of the mean values obtained from control neurons tested in parallel (F_s* and A_s*, respectively). The ability of STI571 to depress nicotinic synaptic function was concentration-dependent, with dose-response studies predicting similar IC_{50} values of 1.0 and 1.8 μM for reducing sEPSC F_s* and A_s*, respectively (Fig. 3, D and E). These results indicate that STI571 depresses frequency and amplitude of α3*-nAChR mediated sEPSCs, thereby suggesting that Abl kinase activity normally sustains the function of α3*-nAChR dependent synapses.

Abl Kinase Inhibition Targets Postsynaptic nAChRs

Because STI571 could depress synaptic transmission by influencing postsynaptic α3*-nAChRs or presynaptic ACh release, quantal components of transmission were analyzed to distinguish between these possibilities. Quantal size is considered the postsynaptic receptor response to transmitter released from a single synaptic vesicle and can be assessed from the average amplitude of mEPSCs recorded in the presence of TTX to block impulse-dependent vesicular release (Johnston and Wu, 1995; Pugh et al., 2010). In control neurons in 4-day CG cultures, α3*-nAChR mediated mEPSCs displayed average amplitudes (a_s) of −13.4 pA and occurred at frequencies (f_s) of 0.3 Hz (Table 2). Consistent with an effect on quantal size, 10 μM STI571 reduced a_s to <50% of that for untreated neurons from the same cultures (Fig. 4A; Table 2). The ability of STI571 to reduce a_s was concentration-dependent, displaying an IC_{50} of ≈2.0 μM (Fig. 4B). STI571 nominally reduced mEPSC frequency (f_s), but the apparent effect was not statistically significant and disappeared entirely when values from treated neurons were normalized to those obtained from controls in the same experiments (f_s*; Fig. 4B; Table 2).

The failure of STI571 to significantly influence mEPSC frequency suggested that any regulation triggered by AFK inhibition would be confined to postsynaptic nAChRs. To assess an additional impact on presynaptic function, as seen for hippocampal neurons (Moresco et al., 2003), we compared

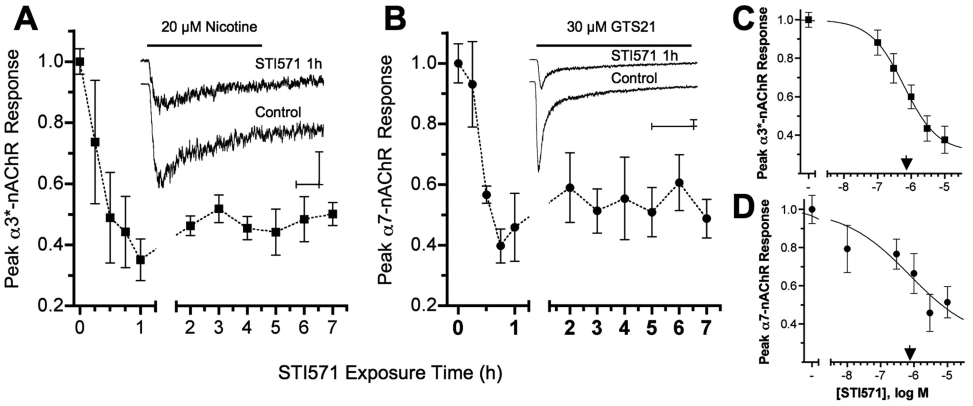

Fig. 2. Abl kinase activity sustains neuronal nAChR function. A and B, Abl kinase inhibition with 10 μM STI571 reduced peak α3*- and α7-nAChR-mediated whole-cell current responses by ≈60% within 1 h. To selectively activate α3*- or α7-nAChR currents, E14 CG neurons were challenged for 1 s either with 20 μM nicotine applied in the presence of 50 nM αBgt (A) or with 20 μM GTS21 (B), respectively. Plots show the time-dependent decline in peak α3*- (■) or α7-nAChR (●) currents divided by membrane capacitance (I^*_{peak}, picoamperes per picofarad) after treatment with 10 μM STI571 relative to untreated controls from the same experiments. Each point in A and B, respectively, represents the mean peak response (± S.E.M.) from STI571-treated neurons tested after the indicated exposure times (n = 5–13 and 5–10 each) relative to untreated control neurons (n = 28 and 26) from the same cultures (N = 8 and 6). The insets show example currents acquired from STI571-treated (10 μM, 1 h) and control neurons, calibration bars indicating 200 pA and 250 ms. C and D, Abl kinase inhibition reduced nAChR responses in a dose-dependent fashion. STI571 applied at increasing concentrations for 1 h progressively reduced peak α3*- (■, C) and α7-nAChR (●, D) responses. Each point in C and D, respectively, represents the mean peak nAChR response (± S.E.M.) from neurons treated with 0.1, 0.3, 1, 3, or 10 μM STI571 (n = 9–11 and 6–10 each) relative to untreated control neurons (n = 9–17 and 8–15 each) tested in the same experiments (N = 5 and 3). The IC_{50} values predicted for α3*- and α7-nAChR inhibition (▼) were 0.6 and 0.7 μM STI571, respectively.

TABLE 1

Abl kinase inhibition with STI571 alters nAChR response parameters

Whole-cell responses mediated by α3*-nAChRs, α7-nAChRs, and GABARs were induced by rapid agonist microperfusion in E14 CG neurons held at −70 mV (see *Materials and Methods* and Fig. 2). I^*_{peak} represents the peak current response relative to the neuronal membrane capacitance. T_{peak} indicates the time from the start of agonist delivery to the current peak. τ_{fast} and τ_{slow} represent the fast and slow exponential time constants of nAChR current decay. Neurons were either treated with STI571 (10 μM, 45–90 min) or sham-treated for the same times with control bathing solution. In this and all tables, parameter values are given as mean ± S.E., with the number of neurons tested in parentheses.

	α3*-nAChR			α7-nAChR				GABA Receptor I^*_{peak}
	I^*_{peak}	T_{peak}	τ_{slow}	I^*_{peak}	T_{peak}	τ_{fast}	τ_{slow}	
	pA/pF	*ms*	*ms*	*pA/pF*	*ms*	*ms*	*ms*	*pA/pF*
Control	−21.6 ± 1.4 (28)	125 ± 12 (21)	3712 ± 401 (20)	−51.6 ± 5.3 (26)	23 ± 1 (22)	44 ± 7 (22)	1087 ± 182 (21)	−102.3 ± 21 (8)
STI571	−9.2 ± 1.2 (22)*	120 ± 15 (16)	2850 ± 425 (13)	−21.1 ± 2.6 (15)*	31* ± 2 (12)	45 ± 9 (11)	1130 ± 379 (11)	−103.0 ± 19 (8)
p Values	< 0.0001	0.79	0.15	< 0.0001	< 0.001	0.93	0.92	0.98

* Parameter values in the STI571-treated group that are significantly different from those in sham-treated controls (P < 0.05, Student's unpaired two-tailed t test).

the average number of vesicles released per presynaptic impulse (mean quantal content, m) for control and STI571-treated neurons. Quantal content was initially estimated from the ratio of average sEPSC to mEPSC amplitudes ($m_s = A_s/a_s$). To more quantitatively assess pre- and postsynaptic function, fascicle stimulation was used to evoke transmission. This approach provided a direct measure of quantal content from the ratio of average eEPSC amplitudes to average mEPSC amplitudes ($m_e = A_e/a_s$) and from the Poisson failure prediction [$m_f = ln\ (N_T/N_0)$] as described previously (Pugh et al., 2010) and under *Materials and Methods* (Fig. 4C). For control neurons, mean quantal content estimates based on these three different approaches were in remarkably good agreement (Table 2). Moreover, fascicle stimulation allowed direct and failure-based estimates of quantal content obtained from the same neurons to be compared, revealing a strong linear correlation between m_e and m_f ($r^2 = 0.98$) with slope ≈1 (data not shown). As expected from its effects on nAChRs and nAChR-mediated sEPSCs and mEPSCs, STI571 treatment reduced evoked EPSC amplitudes (A_e) by ≈60% relative to controls tested in the same experiments (Fig. 4D). Consistent with an effect confined to a postsynaptic site, however, AFK inhibition with 10 μM STI571 failed to alter mean quantal content calculated using either the spontaneous (m_s) or evoked (m_e and m_f) transmission assays (Table 2). The preceding results demonstrate that inhibiting

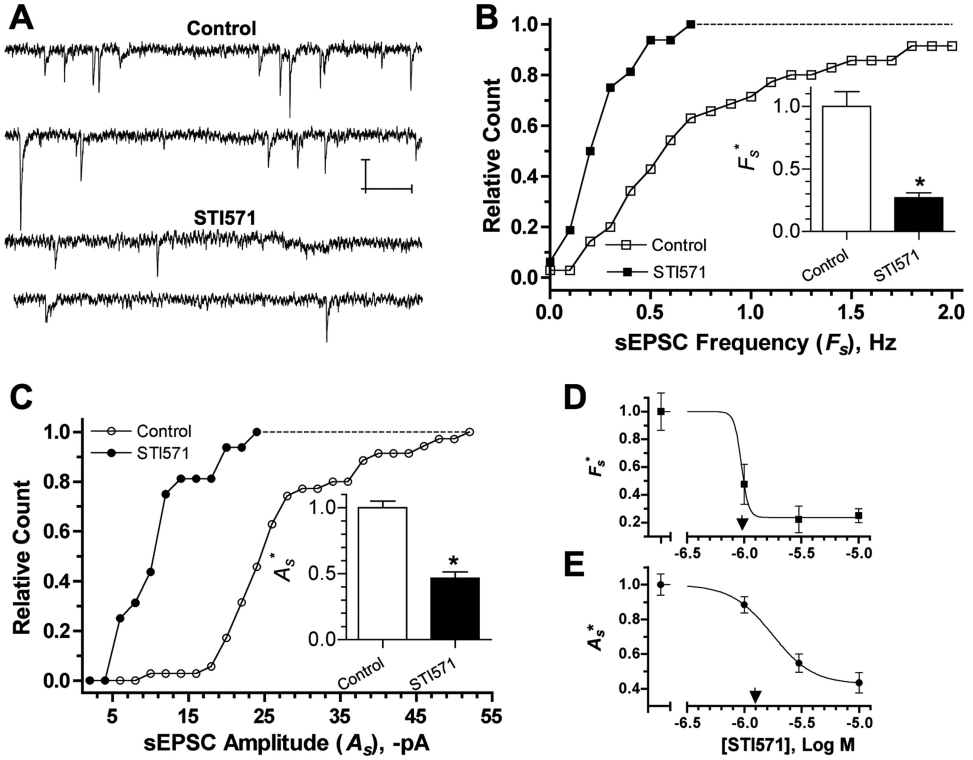

Fig. 3. Abl kinase activity sustains nAChR-mediated synaptic activity. A to C, Abl kinase inhibition with 10 μM STI571 reduced the frequency and amplitude of sEPSCs. A, example whole-cell current records from neurons in sham-treated (Control, top) and STI571-treated (STI571, bottom) 4-day CG cultures, calibration bars depicting 20 pA and 250 ms. B and C, cumulative histograms of mean sEPSC frequencies (F_s, B) and amplitudes (A_s, C) acquired in individual experiments from control neurons (□,○; $N_{T,s}$ = 3495 EPSCs, n = 35 neurons, N = 7 cultures) and neurons treated with 10 μM STI571 (■, ●; $N_{T,s}$ = 529 EPSCs, n = 16 neurons, N = 5 cultures). STI571 treatments of 1 and 24 h gave similar results, and the data have been combined. Inset bar graphs depict relative sEPSC frequencies and amplitudes (F_s* and A_s*, respectively), representing F_s and A_s values normalized to controls from the same experiments (*, $p < 0.05$ by Student's t test). D and E, Abl kinase inhibition reduced synaptic activity in a dose-dependent fashion. STI571 applied for 24 h at increasing concentrations progressively reduced F_s* (■, D) and A_s* (●, E). Each point in D and E represents the F_s* or A_s* value (± S.E.M.) from neurons treated with 1, 3, or 10 μM STI571 (n = 10–14) relative to untreated control neurons (n = 13–17) tested in the same experiments (N = 5). The STI571 concentrations predicted to achieve 50% F_s* and A_s* inhibition (IC_{50}) were 1.0 and 1.8 μM, respectively (arrowheads).

TABLE 2

Abl kinase inhibition with STI571 alters α3*-nAChR mediated synaptic transmission

Spontaneous and evoked synaptic activity was recorded from neurons in 4-day CG cultures. F_s and A_s indicate the frequency and amplitude of sEPSCs. mEPSCs were acquired by blocking impulses with 1 μM TTX. mEPSC frequency and amplitude are indicated by f_s and a_s, respectively, f_s* indicating normalized mEPSC frequency. Quantal content (m) determinations were made based on spontaneous (m_s) and evoked EPSCs (m_e and m_f) as described under *Results*. Values from neurons treated with STI571 (10 μM) for 1 and 24 h have been combined.

	sEPSC		mEPSC			Quantal Content		
	F_s	A_s	f_s	f_s*	a_s	m_s	m_e	m_f
	Hz	*pA*	*Hz*		*pA*			
Control	0.83 ± 0.12 (35)	−27.8 ± 1.5 (35)	0.30 ± 0.11 (19)	1.00 ± 0.13 (19)	−13.4 ± 1.3 (19)	1.9 ± 0.1 (18)	1.7 ± 0.4 (6)	1.5 ± 0.3 (6)
STI571	0.28 ± 0.05 (16)*	−11.9 ± 1.3 (16)*	0.10 ± 0.01 (20)	0.95 ± 0.18 (20)	−6.1 ± 0.1 (20)*	1.9 ± 0.2 (16)	2.3 ± 0.4 (6)	1.3 ± 0.3 (6)
p =	<0.0001	<0.0001	0.06	0.82	<0.0001	0.99	0.27	0.65

* Parameter values in the STI571-treated group that are significantly different from those in sham-treated controls ($P < 0.05$, Student's unpaired two-tailed t test).

Abl kinase activity with STI571 decreases quantal size at nicotinic synapses without affecting basal presynaptic release frequency or impulse-driven quantal content. Because STI571 decreased whole-cell currents from α3*-nAChRs distributed over the entire cell surface (Fig. 2), the results suggest that endogenous Abl kinase activity sustains quantal size by influencing α3*-nAChRs in the postsynaptic membrane.

How Does Abl Kinase Inhibition Reduce nAChR Responses?

The preceding results indicate that inhibiting Abl kinase with STI571 specifically reduces responses generated by the surface population of α3*- and α7-nAChRs, including those α3*-nAChRs restricted to the postsynaptic membrane that mediate synaptic activity. We considered two general mechanisms to explain these actions. The first, based on the observation that STI571 blocks muscle nAChR clustering at the developing neuromuscular junction (Finn et al., 2003), was that STI571 might act to reduce the number of surface α3*- and/or α7-nAChRs or inhibit α3*-nAChR clustering on CG neurons. The second was that STI571 might restrict the function of existing α3*- and α7-nAChRs on the surface of CG neurons.

STI571 Does Not Alter the Density or Distribution of Surface nAChRs. We used confocal microscopy to test the first mechanism, labeling CG cultures with mAb35 to detect surface α3*-nAChRs and with mAbh10 to detect SV2-positive presynaptic terminals (Chen et al., 2001). In images acquired from control neurons, both *z*-stack projections and single *en-face* (surface) optical sections displayed nonuniform mAb35 labeling indicative of α3*-nAChR aggregation into cell surface clusters (Fig. 5, A and B). Values for α3*-nAChR cluster area, density, and fluorescence intensity relative to background ($\Delta F/F_b$) are given in Table 3. Merging adjoining *en-face* optical sections colabeled mAb35 and mAbh10 (Fig. 5C) revealed considerable alignment of α3*-nAChR with SV2-positive presynaptic terminals (Fig. 5D), as quantified by an overall Manders coefficient score of 0.6 (Table 3). The extent of α3*-nAChR localization to the immediate postsynaptic membrane was determined from the portion of each α3*-nAChR cluster aligned with a corresponding SV2-positive presynaptic terminal. The mean area, density, and relative intensity of these synaptic α3*-nAChR puncta are given in Table 3. Overall, STI571 had little effect on the pattern of α3*-nAChR labeling or its alignment with SV2 labeling (Fig. 5, E–H). Specifically, although STI571 treatment (10 μM, 24 h) modestly reduced α3*-nAChR cluster density by 15% ($p = 0.048$), it completely failed to alter the size or intensity of α3*-nAChR clusters, Manders coefficient, or the size, density, or intensity of postsynaptic α3*-nAChR puncta (Table 3). These results suggest that, for nicotinic synapses on CG neurons, AFK activity regulates postsynaptic α3*-nAChR function without influencing their clustering, distribution, or alignment with presynaptic terminals. In addition, the overall surface intensity of mAb35 labeling was unchanged (Table 3) suggesting that the total number of surface α3*-nAChRs was not altered by AFK inhibition with STI571. Results from experiments conducted after 1-h treatment with STI571 (10 μM) were similar and yielded identical conclusions (data not shown). Because STI571 decreased current responses recorded from α3*- and α7-nAChRs distributed over the entire surface of CG neurons isolated at E14 (Fig. 2), we also tested whether AFK inhibition would affect nAChR localization in these neurons. Here we used mAb35 or Alexa Fluor 488-coupled αBgt to label α3*- or α7-nAChRs, respectively (Chen et al., 2001). Similar to the results obtained in culture, the size, density, and intensity of both α3*- and α7-nAChR surface clusters on E14 neurons remained unaltered after STI571 treatment, as was the overall surface labeling intensity for each probe (Supplemental Fig. 1; Supplemental Table 1).

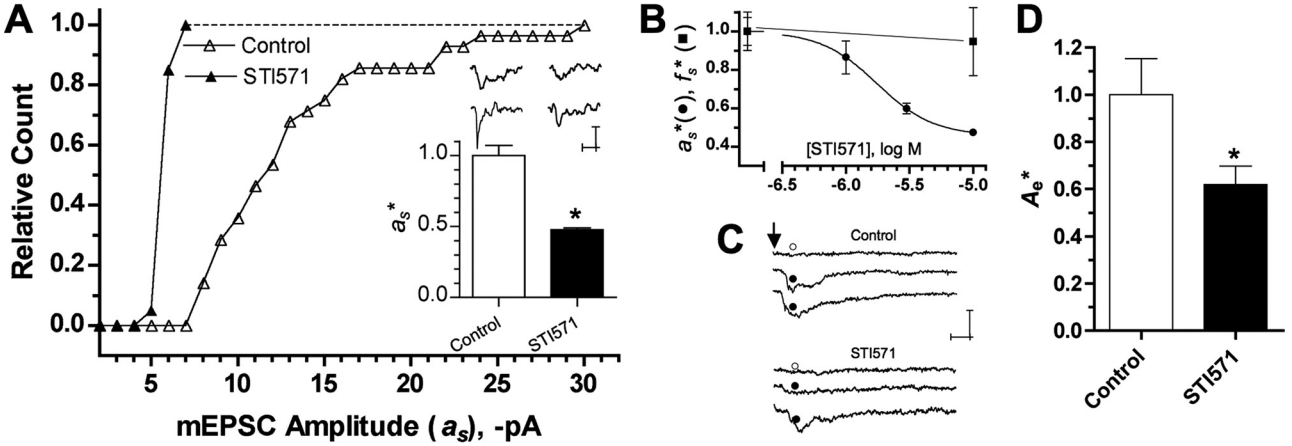

Fig. 4. Abl kinase inhibition selectively reduces the quantal size of nAChR-dependent synaptic events. A, cumulative histogram of mean mEPSC amplitudes (a_s) acquired in the presence of 1 μM TTX from control neurons (△; $n_{T,m}$ = 1153 mEPSCs, n = 19 neurons) and neurons treated with 10 μM STI571 (▲; $n_{T,m}$ = 226 mEPSCs, n = 20 neurons) from the same cultures (N = 5). Treatments with 10 μM STI571 for 1 and 24 h gave similar results, and the data have been pooled. The inset depicts sample mEPSCs (top) and mean amplitudes (bottom) from control and treated neurons. a_s* represents mean mEPSC amplitude for treated relative to sham-treated control neurons from the same experiments (*, $p < 0.05$ by Student's t test). B, Abl kinase inhibition with STI571 applied at increasing concentrations progressively reduced mEPSC amplitude but failed to alter frequency. Each point represents the mEPSC amplitude or frequency (± S.E.M.) from neurons treated with 1, 3, or 10 μM STI571 (n = 9–12) relative to untreated control neurons (n = 3–5) (a_s*, ● or f_s*, ■) assayed in the same experiments (N = 5). The STI571 concentration predicted to achieve 50% inhibition (IC_{50}) of a_s* was ≈2.0 μM. C and D, AFK inhibition reduces the amplitude of stimulus evoked EPSCs. Records in C depict sample eEPSCs (●) and failures (○) from control (top) and STI571-treated neurons after fascicle stimulation (arrow). Calibrations represent 50 pA and 5 ms. Bar graph in D represents cumulative eEPSC amplitudes from STI571-treated neurons (n = 6; 10 μM) relative to untreated control neurons (n = 6) (A_e*) tested in the same experiments (N = 2). *, $p < 0.05$ by Student's t test.

Although the preceding results suggest that AFK inhibition affects nAChR function rather than distribution, we speculated that the imaging methods may not have been sufficiently sensitive to detect STI571-induced changes in surface nAChRs. To address this possibility, the same imaging approaches were used to test the effects of herbimycin A (0.5 μg/ml, 24 h), a broad-spectrum NRTK inhibitor that was previously shown to reduce the number of surface α3*-nAChRs on CG neurons (Haselbeck and Berg, 1996). In contrast with STI571, herbimycin A treatment dramatically reduced the overall intensity of surface α3*-nAChR labeling as well as the density of clusters, whereas the size and intensity of the few remaining surface clusters remained unchanged (Fig. 5, I and J; Table 3). Herbimycin A also greatly reduced presynaptic SV2 labeling, making it difficult to detect synaptic α3*-nAChR puncta in treated cultures (Fig. 5, K and L; Table 3). Although these findings suggest herbimycin A has additional effects on presynaptic components, they are consistent with previous results showing that pan-selective NRTK inhibition with herbimycin A causes a general loss of surface α3*-nAChRs (Haselbeck and Berg, 1996). They further indicate that the imaging approaches used here would have reported changes in nAChR numbers and distribution had they been caused by selectively inhibiting AFKs with STI571. Taken together, the above results indicate that, unlike its role in maintaining muscle nAChR clusters, AFK activity modulates the function of neuronal α3*- and α7-nAChRs without detectably changing their numbers or cell surface distribution.

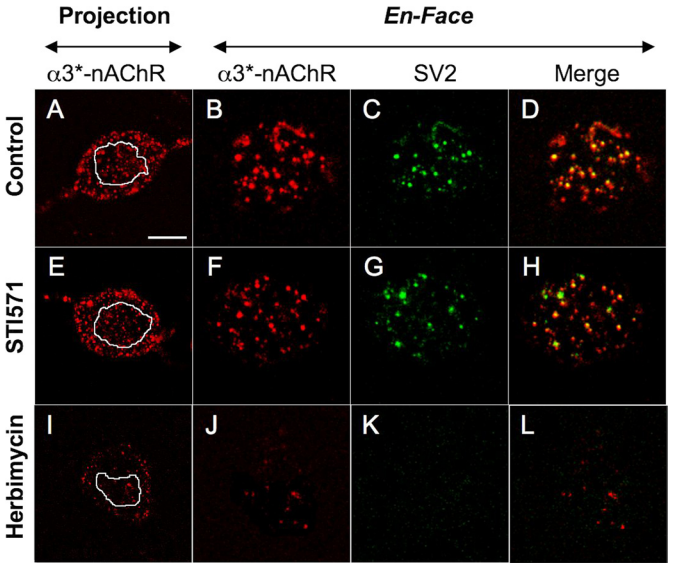

Fig. 5. Abl kinase inhibition fails to alter α3*-nAChR surface distribution or synaptic localization. Confocal images of CG neuron somas from 4-day cultures show α3*-nAChRs (labeled with mAb35, red), SV2-containing presynaptic terminals (labeled with mAbh-10, green), and synaptic sites, where they overlap (yellow). A, E, and I, *z*-stack optical projections from soma midline to top surface reveal an extensive distribution of α3*-nAChRs. The white outlines depict the region of interest (ROI) boundaries of subsequent single *en-face* optical sections. B, F, and J, *en-face* optical sections depict the distribution of α3*-nAChR clusters at the soma surface. C, G, and K, corresponding single *en-face* optical sections depicting the SV2-containing presynaptic terminals. D, H, and L, merged images showing α3*-nAChR clusters colocalized with presynaptic terminals (yellow). Note that compared with untreated controls (A to D), the pattern of α3*-nAChR and SV2 labeling is unaltered in neurons treated with STI571 (10 μM, 24 h; E to H), but drastically different in neurons treated with herbimycin A (0.5 μg/ml, 24 h; I–L). Calibration bar, 10 μm in projection panels; 5 μm in *en-face* panels.

STI571 Influences Nicotinic Signaling by Inhibiting Abl Family Kinases

Neither PDGF nor c-Kit Receptors Are Linked to nAChR Modulation. In addition to AFKs, STI571 targets PDGF-α and -β and c-Kit receptor tyrosine kinases, inhibiting them all with similar potency (IC_{50} = 0.1 to 0.5 μM) (Okuda et al., 2001; Capdeville et al., 2002). In hippocampus, PDGF-β receptors activate Abl, which subsequently inhibits NMDA receptor function (Valenzuela et al., 1996; Beazely et al., 2008). Given this precedent, we tested for PDGFR expression and involvement in regulating nAChR-mediated function. Consistent with their wide distribution in the nervous system (for review, see Valenzuela et al., 1996) PDGFRs were detected in both CG homogenates and neurons (Supplemental Fig. 2, A and B). If the STI571 effects we observed required inhibition of PDGFRs positively linked to nAChRs, then applied PDGF would be expected to enhance nAChR currents, assuming that endogenous PDGFR activation levels are submaximal. To examine this possibility, recombinant PDGF (Sigma-Aldrich) was applied to CG neurons and cultures at 10 nM, the same dose that maximally activated Abl and influenced NMDAR currents in hippocampal neurons (Valenzuela et al., 1996; Beazely et al., 2008). After treatment, however, there were no significant changes in α3*-nAChR currents, sEPSC frequency, or amplitude relative to sham-treated control neurons tested in parallel (Supplemen-

TABLE 3

Abl kinase inhibition with STI571 and broad-spectrum tyrosine kinase inhibition with herbimycin A differentially affect α3*-nAChR distribution

Analysis of confocal images from CG neurons in 4-day cultures immunolabeled with mAb35 and mAbh10 to detect α3*-nAChR clusters and their overlap with SV2-containing presynaptic terminals, respectively. nAChR clusters were identified and analyzed in regions of interest (ROIs) from surface (*en-face*) optical sections as described under *Materials and Methods*. Overall intensity applies to the mean mAb35 (α3*-nAChR) fluorescence intensity within selected *en-face* ROIs; R_m indicates Manders coefficient for α3*-nAChR/SV2 colocalization. Other parameters indicate α3*-nAChR cluster or synaptic puncta size, density, and intensity as indicated in the text. STI571 (top) was applied at 10 μM for 24 h; herbimycin A (bottom) was applied at 0.5 μg/ml for 24 h. Both were compared with separate sham-treated controls from the same experiments.

	α3*-nAChR Labeling				α3*-nAChR/SV2 Overlap			
	Cluster Size	Cluster Density	Cluster Intensity	Overall Intensity	R_m	Puncta Size	Puncta Density	Puncta Intensity
	μm^2	μm^{-2}	$\Delta F/F_b$	$\Delta F/F_b$		μm^2	μm^{-2}	$\Delta F/F_b$
Control (n = 11)	0.24 ± 0.03	0.35 ± 0.02	14.5 ± 0.7	2.6 ± 0.5	0.60 ± 0.04	0.12 ± 0.01	0.17 ± 0.02	18.3 ± 0.7
STI571 (n = 10)	0.29 ± 0.03	0.29* ± 0.02	13.5 ± 0.5	2.2 ± 0.3	0.55 ± 0.05	0.15 ± 0.02	0.16 ± 0.02	17.1 ± 0.5
p Values	0.25	< 0.05	0.26	0.79	0.45	0.20	0.73	0.18
Control (n = 7)	0.22 ± 0.02	0.34 ± 0.01	19.7 ± 1.5	3.5 ± 0.3	N.D.	N.D.	N.D.	N.D.
Herbimycin A (n = 9)	0.14 ± 0.04	0.05 ± 0.01*	16.1 ± 1.2	0.7* ± 0.1	N.D.	N.D.	N.D.	N.D.
p Values	0.10	< 0.0001	0.08	< 0.0001				

N.D., not done.

* Parameter values in the STI571-treated group that are significantly different from those in sham-treated controls ($P < 0.05$, Student's unpaired two-tailed t test).

tal Fig. 2, C–E). The c-Kit receptor tyrosine kinase is expressed widely in the nervous system and in dorsal root ganglion neurons, modulation of neuronal responses by the c-Kit ligand, stem cell factor (SCF; 10 nM, 5 min) is inhibited by STI571 (Milenkovic et al., 2007). To assess a role for c-Kit in modulating α3*-nAChRs, 10 nM recombinant mouse SCF (R&D Systems, Minneapolis, MN) was applied to CG cultures for 5 to 30 min. As with PDGF treatment, however, there was no significant difference in α3*-nAChR responses from SCF-treated neurons (-13.1 ± 1.1 pA/pF, $n = 8$) and sham-treated controls (-16.6 ± 2.3 pA/pF, $n = 8$) tested in parallel ($p > 0.1$). These findings indicate that neither PDGFR nor c-Kit enhances α3*-nAChR-mediated function, thereby suggesting that the inhibitory effects of STI571 on nicotinic receptors and synapses occur via AFKs rather than by coinhibition of endogenous PDGFR or c-Kit.

STI571 Does Not Block nAChRs. STI571 treatment reduced peak agonist-induced α3*- and α7-nAChR current responses as well as α3*-nAChR-mediated EPSCs without appreciably affecting receptor desensitization or activation kinetics (Figs. 2–4; Tables 1 and 2). Because treated neurons were tested in the presence of STI571, such reductions could arise if STI571 competed for the agonist binding site on α3*- and α7-nAChRs or blocked their respective channels. If STI571 acted as a competitive inhibitor, it would be expected to shift apparent nAChR affinity (EC_{50}), such that higher agonist concentrations would be required to achieve the same maximal responses in treated relative to control neurons. We therefore assayed α3*- and α7-nAChR whole-cell responses from acutely dissociated CG neurons (as in Fig. 2) using a range of nicotine and GTS21 concentrations and compared EC_{50} values for control and STI571-treated neurons. In both cases, maximal α3*- and α7-nAChR responses were induced by 100 μM nicotine and 30 μM GTS21, respectively, and those from STI571-treated neurons were reduced to $\approx$50% of controls tested in parallel, without a significant shift in EC_{50} values (Fig. 6, A and B). These findings indicate that STI571 does not compete with nicotine or GTS21 for the agonist binding sites on α3*- or α7-nAChRs, respectively. To test the possibility that STI571 functions as an open-channel blocker, we measured pairs of nAChR responses to agonist application. If STI571 acted as an open channel blocker, it would occupy sites within the channel pore during receptor activation for the first response (R1) and make the second response amplitude (R2) smaller than untreated conditions. To test this possibility for α3*-nAChRs, responses to 20 μM nicotine (in the presence of 100 nM αBgt) were recorded with a 30-s interval between R1 and R2 (Fig. 6B). As expected, STI571 treatment (10 μM, 1 h) reduced both α3*-nAChR R1 and R2 relative to corresponding responses from untreated controls tested in parallel. The R2/R1 ratios in STI571 treated and control neurons were indistinguishable (Fig. 6C), however, a finding that is inconsistent with a channel block mechanism. A modified procedure was required to assess pairs of α7-nAChR responses. In this case, the prolonged desensitization of α7-nAChRs required much longer intervals between R1 and R2, which frequently destabilized the whole-cell patch configuration. To overcome this problem, mean α7-nAChR responses to GTS-21 (30 μM) were collected from control and STI571-treated neurons (R1) and then from a set of different control and STI571-treated neurons from the same platings 10 min after 1-s exposure to GTS-21 (R2). Once again, the findings were inconsistent with STI571 acting as a channel blocker because STI571 significantly reduced α7-nAChR R1 and R2, but the R2/R1 ratios for STI571-treated and control neurons were indistinguishable (Fig. 6C). These pharmacological blockade experiments indicate that STI571 reduces nAChR responses by inhibiting AFK activity rather than by acting as a competitive inhibitor or an open channel blocker of neuronal nAChRs.

STI571 Does Not Alter F-Actin Organization. AFKs are thought to mediate nAChR clustering in muscle by a mechanism involving obligatory MuSK phosphorylation, and subsequent AFK binding of filamentous actin (F-actin) to create a stabilized postsynaptic scaffold (Wang et al., 2001; Finn et al., 2003). Indeed, neuronal α7-nAChR and muscle nAChR clusters can be disrupted by latrunculin-A, an inhibitor F-actin polymerization (Dai et al., 2000; Shoop et al.,

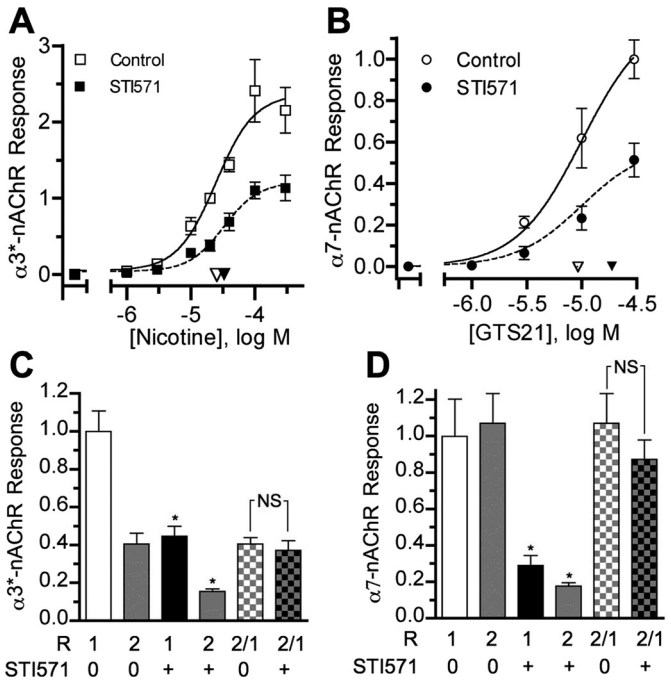

Fig. 6. STI571 reduces nAChR responses without directly inhibiting nAChRs. A and B, testing for competition with nAChR agonists. Increasing concentrations of nicotine applied to E14 CG neurons in the presence of αBgt to selectively activate α3*-nAChRs (A) or GTS21 to selectively activate α7-nAChRs (B) induced dose-dependent peak responses (see legend to Fig. 2) that were consistently smaller in neurons treated with STI571 (■, ●) relative to controls (□, ○). *y*-Axes indicate peak nAChR responses induced by varying concentrations of nicotine relative to 20 μM nicotine (A) or varying concentrations of GTS-21 relative to 30 μM GTS-21 (B); responses from STI571-treated neurons are normalized to untreated controls tested in parallel. The respective EC_{50} values for control and STI571-treated neurons (▽ and ▼) were 2.8 and 3.3 μM nicotine for α3*-nAChRs and 9.1 and 18.9 μM GTS-21 for α7-nAChRs. For both receptor subtypes, the 95% confidence intervals of EC_{50} values for control and treated neurons overlapped (not shown), indicating that STI571 does not compete with α3*- or α7-nAChR agonists. C and D, testing for block of open nAChR channels. Peak α3*- and α7-nAChRs responses were generated in control and STI571-treated E14 CG neurons by paired applications of 20 μM nicotine (separated by 30-s intervals; C) or 30 μM GTS-21 (separated by 10-min intervals; D), respectively (see *Results* and legend to Fig. 2). For α3*- and α7-nAChRs, STI571 (+) reduced both the first and second responses (1 and 2) relative to corresponding responses from untreated controls (0; *, $p < 0.05$, Student's *t* test) but response ratios (2/1) were not detectably different (NS indicates $p > 0.05$, Student's *t* test). *y*-Axes indicate normalized peak nAChR responses obtained with 20 μM nicotine (B) or 30 μM GTS-21 (D) or the corresponding 2/1 ratios.

2000). Previous findings indicate that the Abl2 C-terminal actin binding regions are distinct from the kinase domain (Pendergast, 2002) and necessary and sufficient for actin binding and bundling (Wang et al., 2001). Moreover, MuSK has roles in the nervous system that are different from those in muscle (Garcia-Osta et al., 2006). It was therefore anticipated that inhibiting kinase activity with STI571 would fail to influence F-actin structure, consistent with its inability to change nAChR distribution. To test this idea, we visualized F-actin in CG neurons using rhodamine-phalloidin (Shoop et al., 2000). In both acutely dissociated and cultured CG neurons, STI571 treatment (10 μM, 24 h) failed to significantly change F-actin cluster size, intensity, or density (Supplemental Fig. 3; Supplemental Table 2), suggesting that inhibiting Abl kinase activity has no effect on C-terminal links to the CG neuron F-actin cytoskeleton. To address the possibility that STI571 caused subtle F-actin perturbations undetected by rhodamine-phalloidin that might nevertheless affect nAChR function, we assessed the ability of STI571 to affect α3*-nAChR responses after preventing actin depolymerization with jasplakinolide (Invitrogen) as described previously (Shoop et al., 2000). No evidence was found to support this possibility, however, because α3*-nAChR current responses in CG neurons preincubated with jasplakinolide were still significantly reduced by >40% after STI571 treatment (data not shown). Taken together, these findings support the idea that STI571 reduces nAChR-mediated signaling in CG neurons by reducing endogenous AFK kinase activity and not by acting via PDGFR, c-Kit, nAChR blockade, or by perturbing the F-actin cytoskeleton.

Discussion

Abelson family kinases are well known from their role in CML, but they are also regulators of normal cellular processes. Studies using *Abl*(−/−) mice and STI571 have demonstrated that Abl tyrosine kinase activity maintains vital functional components of chemical synapses in brain (Moresco et al., 2003; de Arce et al., 2010) and muscle (Finn et al., 2003). Here, STI571 restricted the function of neuronal nAChRs and nAChR-mediated synapses on CG neurons by obligatory inhibition of Abl tyrosine kinase activity. Several lines of evidence support this conclusion. First, STI571 inhibited AFKs in the CG because its application nearly abolished endogenous tyrosine phosphorylation of CrkII, a specific AFK substrate (Feller et al., 1994). Second, STI571 reduced nAChR function and tyrosine kinase activity in parallel, displaying submicromolar potencies for inhibiting α3*- and α7-nAChR currents that were similar to those found previously for inhibiting Abl tyrosine kinase activity (Okuda et al., 2001; Capdeville et al., 2002). Third, STI571 did not detectably alter the F-actin cytoskeleton and retained its ability to reduce nAChR responses after stabilizing actin with jasplakinolide. Fourth, although STI571 inhibits PDGFR and c-Kit at concentrations similar to those at which it inhibit AFKs (Okuda et al., 2001; Capdeville et al., 2002), their respective ligands failed to enhance nAChR currents. Assuming endogenous PDGFR and c-Kit are active at submaximal levels, this finding indicates that neither contributes to the actions of STI571 observed here. Fifth, STI571 did not directly inhibit nAChRs, because it failed to act as a competitive antagonist or open channel blocker. These considerations support the conclusion that STI571 inhibits endogenous Abl tyrosine kinase activity, which normally sustains α3*- and α7-nAChR function and nAChR-mediated EPSCs. It is possible that Abl kinase activity similarly influences other nAChR subtypes, such as those containing $\alpha4\beta2$ subunits that are prominent in the central nervous system. Because STI571 is expected to inhibit the kinase activity of Abl1 and Abl2, however, we are unable to determine whether one or both are relevant to nAChR modulation.

The observed regulation of postsynaptic function contrasts with previous results (Moresco et al., 2003) where the paired-pulse facilitation ratio, an indirect measure of presynaptic function, was reduced in hippocampal slices from *Abl1*(−/−) and *Abl2*(−/−) mice, and mimicked by STI571. In CG neuron cultures, however, where STI571 reduced the frequency and amplitude of α3*-nAChR-mediated sEPSCs, the locus was postsynaptic, because STI571 reduced postsynaptic mEPSC amplitude (quantal size) but, in the same experiments, failed to alter either mEPSC frequency or mean quantal content, two established measures of presynaptic function (Johnston and Wu, 1995). The reduction in quantal size and EPSC amplitudes would lower suprathreshold activity throughout the culture network, reducing sEPSC frequency as was observed. In CG cultures, synaptic transmission is mediated largely by α3*-nAChRs, because α7-nAChR mediated EPSCs are rare and α7 subunit mRNA is expressed at low levels (Chen et al., 2001). In vivo, the CG is composed of postganglionic choroid and ciliary neurons and α3*-nAChRs play a similar dominant role in mediating transmission to choroid neurons, whereas for ciliary neurons, both receptor subtypes participate (Dryer, 1994; Ullian et al., 1997). Thus the ability of STI571 to reduce α3*- and α7-nAChR currents suggests that in vivo Abl kinase activity will influence synapses mediated by the two receptor subtypes on both classes of postganglionic neurons.

Finding that AFKs influence neuronal nAChR function also contrasts with results showing that nAChR clusters are disrupted in mouse myotubes after STI571 treatment (Finn et al., 2003). In dissociated CG neurons, Abl kinase inhibition with STI571 failed to alter the size, density, or intensity of either α3*- or α7-nAChR clusters. A similar pattern prevailed in CG cultures for α3*-nAChRs, which mediate the bulk of synaptic transmission (Chen et al., 2001; Pugh et al., 2010). Moreover, treating the cultures with STI571 had no detectable effect on α3*-nAChR puncta aligned with presynaptic SV2-positive terminals, indicating an unperturbed synaptic cytoarchitecture. These negative findings were not due to insufficient resolution, because the broad-spectrum tyrosine kinase inhibitor herbimycin A, previously shown to reduce levels of surface α3*-nAChRs (Haselbeck and Berg, 1996), nearly abolished α3*-nAChR clusters. The disparate results can be explained by considering that mechanisms controlling nAChR clustering and cytoskeletal anchoring in muscle do not apply in neurons. In muscle, MuSK activates rapsyn to trigger nAChR clustering and AFKs stabilize the clusters via reciprocal tyrosine phosphorylation of MuSK. The resulting Abl-MuSK interaction is presumed to trigger F-actin polymerization involving Abl C-terminal actin binding domains that "stabilize clusters through induction of a synaptic actin scaffold" (Finn et al., 2003). Although MuSK is present in the nervous system and autonomic neurons contain rapsyn transcripts, neither appears to be involved in

normal nAChR clustering or anchoring (Burns et al., 1997; Feng et al., 1998; Garcia-Osta et al., 2006). Instead, Abl kinase activity seems to influence nAChR function, whereas PDZ-domain-containing postsynaptic density (PSD) proteins in the PSD95 family that anchor receptors by interacting with intermediates to form cytoskeletal links seem likely effectors controlling nAChR anchoring (see discussion below). In summary, our results indicate that Abl kinase activity is important for sustaining nAChR function in CG neurons and by doing so enhances postsynaptic nAChR-mediated neurotransmission without affecting presynaptic mechanisms or synaptic cytoarchitecture as found previously in hippocampus and muscle, respectively.

Aspects of nAChR function sensitive to Abl kinase activity are unknown. Because STI571 reduced peak agonist-induced nAChR currents without affecting other response parameters, AFKs probably do not affect receptor activation or agonist-induced desensitization. Properties more likely to be influenced are nAChR affinity, single channel conductance, open time, and/or availability to function. It is interesting that inhibiting the activity of Src-family NRTKs was previously shown to reduce chromaffin cell α3*-nAChR currents (Wang et al., 2004) to an extent similar to that seen here. Because inhibiting protein-tyrosine phosphatase (PTPase) activity enhanced α3*-nAChR currents, the authors suggested that "the equilibrium between the activities of SFKs and PTPases favors the PTPases, thereby maintaining the AChR in an inactive state." A similar kinase-phosphatase equilibrium could apply for the Abl kinase-dependent regulation of nAChR currents, because CG neurons express a large surface population of inactive α3*-nAChRs that can be rapidly mobilized into an active state (Margiotta et al., 1987; Nai et al., 2003), a process that is probably triggered by protein phosphorylation (Pardi and Margiotta, 1999).

Phosphorylation substrate(s) relevant to influencing α7 and α3*-nAChR function are also unknown. To determine whether nAChRs themselves are possible targets, we examined the amino acid composition of intracellular regulatory domains between membrane-spanning regions 3 and 4 (M3–M4) in their constituent subunits (α7, α3, α5, β4, and β2) for potential Abl tyrosine phosphorylation sites. Using a group-based kinase prediction system tool (GPS 2.0; Xue et al., 2008) at high stringency to minimize false positives, tyrosine residues suitable for Abl phosphorylation were predicted in the M3–M4 cytoplasmic loop of α3 and β2 subunits but not in α5, α7 or β4 subunits. It is noteworthy that the site identified in β2 at Tyr381 (Y-A-N-P) conforms to a minimal Abl kinase consensus motif {Y-X_{2-3}-(P/F)} that is also present in CrkII at Tyr221 (Y-A-Q-P) and phosphorylated by Abl1 (Feller et al., 1994; Cujec et al., 2002). Thus, Abl tyrosine kinase activity could modulate α3*-nAChR function by direct tyrosine phosphorylation of one or more of its constituent subunits. Other experiments suggest that PSD proteins are targets interposed between AFKs and nAChRs. PSD-95 is known to support AMPA receptor-mediated synaptic function and retention (El-Husseini et al., 2000; Béïque et al., 2006) and associates with Abl1 in hippocampus. STI571 disrupts PSD-95 clustering at these sites, and blocks Abl1-mediated consensus phosphorylation of PSD-95 at Y533 (Y-A-*R*-P) in HEK cells (de Arce et al., 2010). Likewise, α3*-nAChRs associate with PSD-95 in CG neurons, and expression of CRIPT to block a critical PDZ domain drastically reduced subsequent α3*-nAChR mediated sEPSCs (Conroy et al., 2003). This effect was associated with a loss of PSD-95 protein family clusters, but as with STI571 treatment, α3*-nAChR clusters were surprisingly unaffected. The authors concluded that by abolishing PSD-95 clusters, CRIPT may have altered the alignment of presynaptic terminals with postsynaptic α3*-nAChRs. Because colocalization experiments like those conducted here were not performed, another explanation is that CRIPT blocks an AFK-PSD association necessary to sustain the function of synaptic α3*-nAChRs. Although these are intriguing possibilities, further experiments are required to determine whether Abl kinase activity controls neuronal nicotinic signaling by direct phosphorylation of α3*-nAChRs or by indirect actions mediated via phosphorylation of PSD proteins or other intermediate effectors.

Finally, STI571 has been an enormously successful cancer therapy because it targets and inhibits the Bcr-Abl fusion protein and mutated c-Kit tyrosine kinases that are constitutively active in CML and gastrointestinal stromal tumors, respectively. As mentioned and shown above, STI571 applied at equivalent doses also inhibits physiologically relevant nononcogenic tyrosine kinases (c-Kit, PDGFR, and AFKs), and this cross-specificity may be responsible for some of its nontherapeutic side effects (http://www.nlm.nih.gov/medlineplus/druginfo). Other drugs have been developed that are more potent (nilotinib; Novartis) or have different cross-specificity (dasatinib, Bristol-Myers Squibb Co., Stamford, CT) and may reduce some of the side effects. Despite such advances, our study indicates that STI571 reduces autonomic nAChR function and nAChR-mediated synaptic transmission specifically by inhibiting Abl tyrosine kinase activity. Thus even drugs that more potently and perfectly target AFKs may still cause some of the same prominent side effects associated with STI571 (nausea, vomiting, diarrhea, muscle pain/cramps) because these all point to an underlying autonomic dysfunction.

Acknowledgments

We thank Dr. Phyllis Pugh for helpful advice and Novartis for providing STI571.

Authorship Contributions

Participated in research design: Jayakar and Margiotta.
Conducted experiments: Jayakar and Margiotta.
Contributed new reagents or analytic tools: Margiotta.
Performed data analysis: Jayakar and Margiotta.
Wrote or contributed to the writing of the manuscript: Jayakar and Margiotta.
Other: Margiotta acquired funding for the research.

References

Beazely MA, Weerapura M, and MacDonald JF (2008) Abelson tyrosine kinase links PDGFbeta receptor activation to cytoskeletal regulation of NMDA receptors in CA1 hippocampal neurons. *Mol Brain* **1:**20.

Béïque JC, Lin DT, Kang MG, Aizawa H, Takamiya K, and Huganir RL (2006) Synapse-specific regulation of AMPA receptor function by PSD-95. *Proc Natl Acad Sci USA* **103:**19535–19540.

Burns AL, Benson D, Howard MJ, and Margiotta JF (1997) Chick ciliary ganglion neurons contain transcripts coding for acetylcholine receptor-associated protein at synapses (rapsyn). *J Neurosci* **17:**5016–5026.

Capdeville R, Buchdunger E, Zimmermann J, and Matter A (2002) Glivec (STI571, imatinib), a rationally developed, targeted anticancer drug. *Nat Rev Drug Discov* **1:**493–502.

Charpantier E, Wiesner A, Huh KH, Ogier R, Hoda JC, Allaman G, Raggenbass M, Feuerbach D, Bertrand D, and Fuhrer C (2005) Alpha7 neuronal nicotinic acetylcholine receptors are negatively regulated by tyrosine phosphorylation and src-family kinases. *J Neurosci* **25:**9836–9849.

Chen M, Pugh PC, and Margiotta JF (2001) Nicotinic synapses formed between chick

ciliary ganglion neurons in culture resemble those present on the neurons in vivo. *J Neurobiol* **47:**265–279.
Conroy WG, Liu Z, Nai Q, Coggan JS, and Berg DK (2003) PDZ-containing proteins provide a functional postsynaptic scaffold for nicotinic receptors in neurons. *Neuron* **38:**759–771.
Corbin AS, Buchdunger E, Pascal F, and Druker BJ (2002) Analysis of the structural basis of specificity of inhibition of the Abl kinase by STI571. *J Biol Chem* **277:** 32214–32219.
Cujec TP, Medeiros PF, Hammond P, Rise C, and Kreider BL (2002) Selection of v-abl tyrosine kinase substrate sequences from randomized peptide and cellular proteomic libraries using mRNA display. *Chem Biol* **9:**253–264.
Dai Z, Luo X, Xie H, and Peng HB (2000) The actin-driven movement and formation of acetylcholine receptor clusters. *J Cell Biol* **150:**1321–1334.
de Arce KP, Varela-Nallar L, Farias O, Cifuentes A, Bull P, Couch BA, Koleske AJ, Inestrosa NC, and Alvarez AR (2010) Synaptic clustering of PSD-95 is regulated by c-Abl through tyrosine phosphorylation. *J Neurosci* **30:**3728–3738.
Dryer SE (1994) Functional development of the parasympathetic neurons of the avian ciliary ganglion: a classic model system for the study of neuronal differentiation and development. *Prog Neurobiol* **43:**281–322.
El-Husseini AE, Schnell E, Chetkovich DM, Nicoll RA, and Bredt DS (2000) PSD-95 involvement in maturation of excitatory synapses. *Science* **290:**1364–1368.
Feller SM, Knudsen B, and Hanafusa H (1994) c-Abl kinase regulates the protein binding activity of c-Crk. *EMBO J* **13:**2341–2351.
Feng G, Steinbach JH, and Sanes JR (1998) Rapsyn clusters neuronal acetylcholine receptors but is inessential for formation of an interneuronal cholinergic synapse. *J Neurosci* **18:**4166–4176.
Finn AJ, Feng G, and Pendergast AM (2003) Postsynaptic requirement for Abl kinases in assembly of the neuromuscular junction. *Nature Neuroscience* **6:**717–723.
Garcia-Osta A, Tsokas P, Pollonini G, Landau EM, Blitzer R, and Alberini CM (2006) MuSK expressed in the brain mediates cholinergic responses, synaptic plasticity, and memory formation. *J Neurosci* **26:**7919–7932.
Haselbeck RC and Berg DK (1996) Tyrosine kinase inhibitors alter composition of nicotinic receptors on neurons. *Journal of Neurobiology* **31:**404–414.
Hilgenberg LG and Smith MA (2004) Agrin signaling in cortical neurons is mediated by a tyrosine kinase-dependent increase in intracellular Ca^{2+} that engages both CaMKII and MAPK signal pathways. *J Neurobiol* **61:**289–300.
Johnston D and Wu SM (1995) *Foundations of Cellular Neurophysiology*, The MIT Press, Cambridge.
Koleske AJ, Gifford AM, Scott ML, Nee M, Bronson RT, Miczek KA, and Baltimore D (1998) Essential roles for the Abl and Arg tyrosine kinases in neurulation. *Neuron* **21:**1259–1272.
Margiotta J and Pugh P (2004) Nicotinic acetylcholine receptors in the nervous system, in *Molecular and Cellular Insights to Ion Channel Biology* (Maue RA ed), pp 269–302. Elsevier B.V., Amsterdam.
Margiotta JF, Berg DK, and Dionne VE (1987) Cyclic AMP regulates the proportion of functional acetylcholine receptors on chicken ciliary ganglion neurons. *Proc Natl Acad Sci USA* **84:**8155–8159.
Milenkovic N, Frahm C, Gassmann M, Griffel C, Erdmann B, Birchmeier C, Lewin GR, and Garratt AN (2007) Nociceptive tuning by stem cell factor/c-Kit signaling. *Neuron* **56:**893–906.
Moresco E, Scheetz A, Bornmann W, Koleske A, Fitzsimonds R (2003) Abl family nonreceptor tyrosine kinases modulate short-term synaptic plasticity. *J Neurophysiology* **89:**1678–1687.
Nai Q, McIntosh JM, and Margiotta JF (2003) Relating neuronal nicotinic acetylcholine receptor subtypes defined by subunit composition and channel function. *Mol Pharmacol* **63:**311–324.
Nashmi R, Xiao C, Deshpande P, McKinney S, Grady SR, Whiteaker P, Huang Q, McClure-Begley T, Lindstrom JM, Labarca C, et al. (2007) Chronic nicotine cell specifically upregulates functional alpha4* nicotinic receptors: basis for both tolerance in midbrain and enhanced long-term potentiation in perforant path. *J Neurosci* **27:**8202–8218.
Newhouse PA and Kelton M (2000) Nicotinic systems in central nervous systems disease: degenerative disorders and beyond. *Pharm Acta Helv* **74:**91–101.
Okuda K, Weisberg E, Gilliland DG, and Griffin JD (2001) ARG tyrosine kinase activity is inhibited by STI571. *Blood* **97:**2440–2448.
Pardi D and Margiotta JF (1999) Pituitary adenylate cyclase-activating polypeptide activates a phospholipase C-dependent signal pathway in chick ciliary ganglion neurons that selectively inhibits α7-containing nicotinic receptors. *J Neurosci* **19:**6327–6337.
Pendergast AM (2002) The Abl family kinases: mechanisms of regulation and signaling. *Adv Cancer Res* **85:**51–100.
Pugh PC, Jayakar SS, and Margiotta JF (2010) PACAP/PAC1R signaling modulates acetylcholine release at neuronal nicotinic synapses. *Molecular and Cellular Neuroscience* **43:**244–257.
Shoop RD, Yamada N, and Berg DK (2000) Cytoskeletal links of neuronal acetylcholine receptors containing α7 subunits. *J Neurosci* **20:**4021–4029.
Sirvent A, Benistant C, and Roche S (2008) Cytoplasmic signalling by the c-Abl tyrosine kinase in normal and cancer cells. *Biol Cell* **100:**617–631.
Ullian EM, McIntosh JM, and Sargent PB (1997) Rapid synaptic transmission in the avian ciliary ganglion is mediated by two distinct classes of nicotinic receptors. *J Neurosci* **17:**7210–7219.
Valenzuela CF, Xiong Z, MacDonald JF, Weiner JL, Frazier CJ, Dunwiddie TV, Kazlauskas A, Whiting PJ, and Harris RA (1996) Platelet-derived growth factor induces a long-term inhibition of *N*-methyl-D-aspartate receptor function. *J Biol Chem* **271:**16151–16159.
Vernino S, Hopkins S, and Wang Z (2009) Autonomic ganglia, acetylcholine receptor antibodies, and autoimmune ganglionopathy. *Auton Neurosci* **146:**3–7.
Wang K, Hackett JT, Cox ME, Van Hoek M, Lindstrom JM, and Parsons SJ (2004) Regulation of the neuronal nicotinic acetylcholine receptor by SRC family tyrosine kinases. *J Biol Chem* **279:**8779–8786.
Wang Y, Miller AL, Mooseker MS, and Koleske AJ (2001) The Abl-related gene (Arg) nonreceptor tyrosine kinase uses two F-actin-binding domains to bundle F-actin. *Proc Natl Acad Sci USA* **98:**14865–14870.
Xue Y, Ren J, Gao X, Jin C, Wen L, and Yao X (2008) GPS 2.0, a tool to predict kinase-specific phosphorylation sites in hierarchy. *Mol Cell Proteomics* **7:**1598–1608.
Zhou X, Nai Q, Chen M, Dittus JD, Howard MJ, and Margiotta JF (2004) Brain-derived neurotrophic factor and trkB signaling in parasympathetic neurons: relevance to regulating α7-containing nicotinic receptors and synaptic function. *J Neurosci* **24:**4340–4350.

Address correspondence to: Dr. Joseph F. Margiotta, University of Toledo College of Medicine, Department of Neurosciences, Mail Stop 1007, Block HS 108, 3000 Arlington Ave., Toledo, OH 43614-5804. E-mail: joseph.margiotta@utoledo.edu